Volume 7, Issue 6, 2017, 2295 - 2299 ISSN 2069-5837

Biointerface Research in Applied Chemistry

www.BiointerfaceResearch.com

Original Research Article Open Access Journal

Received: 21.11.2017 / Revised: 13.12.2017 / Accepted: 14.12.2017 / Published on-line: 15.12.2017

Mullite ceramics acid corrosion kinetics as a function of gel homogeneity

Stanislav Kurajica [1], Vilko Mandić [1,*], Lidija Ćurković [2]

[1] University of Zagreb, Faculty of Chemical Engineering and Technology, Marulićev trg 19, HR-10000 Zagreb, Croatia

[2] University of Zagreb, Faculty of Mechanical Engineering and Naval Architecture, Ivana Lučića 5, HR-10000 Zagreb, Croatia

*corresponding author e-mail address: ***vmandic@fkit.hr***

ABSTRACT

Using the sol-gel synthesis, premullite gels with different levels of homogeneity, so called monophasic and diphasic gels, were prepared. Gels thermal transformations to mullite ceramics, as well as structural features of ceramic samples were characterized. Gels were processed into mullite ceramics at 1600°C/4h. The occurrence of glassy phase was predominately evidenced in ceramics originating from diphasic gel, while that originating from monophasic gel showed greater porosity. The behaviour of ceramics during corrosion in aqueous nitric acid solutions was evaluated by the amount of eluted ions. Both samples yield low corrosion rates with corrosion kinetics following parabolic function. In comparison with nominal composition the eluates contain higher Si^{4+}/Al^{3+} ratio as a consequence of the leaching of the glassy phase. However, due to a greater porosity the ceramics derived from monophasic gels show higher corrosion rate.

Keywords: *Mullite, corrosion, transmission electron microscopy, inductively coupled plasma-optical emission spectrometry, kinetics*

1. INTRODUCTION

Mullite, $Al^{VI}_2(Al^{IV}_{2+2x}Si_{2-2x})O_{10-x}$, where x is between 0.2 and 0.9, displays importance as a material for both traditional and advanced ceramics on behalf of its favourable thermal and mechanical properties [1]. Mullite ceramic is widely applied for structural or hostile-environment-protective coating materials primarily on behalf of its good creep resistance at high temperatures, but also intrinsic high strength, low thermal expansion and good chemical stability [2-4]. In order to produce mullite ceramics of high purity, homogeneity and lower processing temperatures, a sol-gel synthesis is often applied to fabricate mullite [5]. Moreover, colloidal processing enables low-cost approach for producing uniform, thick ceramic coatings on complex-shaped components via a simple dip coating process [6]. Premullite gels obtained by sol–gel procedure are usually classified into two types according to system homogeneity. Monophasic gels show molecular homogeneity and direct amorphous-to-mullite crystallization at ~980°C, while diphasic gels show reduced but still nanometer level of homogeneity and amorphous-to-mullite crystallization above 1150°C over intermediate spinel phase crystallizing at ~980°C. The DTA curve of such diphasic gel is characterized by a strong exotherm at ~980°C and a weaker one above 1150°C [7].

Corrosion is cause of a considerable damage in many high temperature applications where mullite is employed. Therefore, mullite corrosion resistance is a very important performance criterion [8]. Beside corrosive atmospheres mullite ceramics components often have to withstand high temperatures. Mullite does well here, as it is well known mullite displays low high-temperature creep [8].

Chemical resistance of ceramics is understood as its capacity to withstand a destructive action of aggressive media (gases, solution of acids, bases and salts, sea water, melts, etc.) [9]. The study of corrosion resistance of ceramics in various aggressive media enables prediction of final service properties in these media. The corrosion of ceramics proceeds either as chemical reaction between the ceramic material components and the processing medium elements, or as ceramic material components dissolution in the processing medium [9]. Corrosion rate is usually expressed through corrosion rate const. Stanislav ant, k. In most simple case when corrosion rate obeys linear rate law, k is given as a total amount of species released into the solution (e.g. in grams) per surface area of sample in contact with solution (e.g. in cm^2) and duration of sample contact with solution (e.g. in hours).

The corrosion of mullite in water vapour [10-12], hot gas environment, [13-14] alkali vapour [15-16] and salts [17] has been widely investigated. On the other hand, research of acid corrosion properties of mullite ceramics has not received much attention. The evaluation of the of corrosion process of ceramics is normally performed by analysis of the total weight loss of specimens immersed in corrodent. The chemical stability could be determined more precisely by analysis of eluted ions amounts. In this study we aim to examine the corrosion behaviour of monophasic (MP) and diphasic (DP) mullite ceramics, derived from gels, in nitric acid. Elements eluted after immersion in HNO_3 aqueous solution of various concentrations have been measured. Sintered samples were characterised prior and after immersion, where the microstructure, morphology and chemical composition were considered.

2. EXPERIMENTAL SECTION

The premullite gels were prepared by dissolving $Al(NO_3)_3{\cdot}9H_2O$ (p.a., Kemika, Croatia) in ethanol (monophasic gel) or water (diphasic gel). The nitrate:ethanol (96% purity, Kemika, Croatia) molar ratio was 1:9, while nitrate:water was

1:28. The solutions were stirred and refluxed at 60°C for 1 day. Tetraethoxysilane (98% purity, Merck, Germany) was mixed with ethanol (TEOS:ethanol molar ratio 1:9) and stirred at room temperature for 1 h. The TEOS mixture was added drop-wise to the nitrate solutions. The molar ratio of Al:Si in both samples was 3:1 (stoichiometric 3:2 mullite). The mixture was stirred at 60°C for 8 days under reflux. The gel was dried 1 day under 150 W IR lamp, further 3 days at 110°C in laboratory drier and subsequently calcined at 700°C for 2 h to decompose the organics and remove the volatiles in a laboratory box-furnace. Derived mass was wet-grinded in a planetary mill at 200 rpm for 2 h (2-propanol as a milling media) to fine powder. Grinded samples were ambient-dried. Remaining propanol was removed by another calcification at 700°C for 2 h. The mullite powders were then uniaxially pressed (Paul Webber GmbH) with help of die into pellets with diameter of 10 mm (2 g of premullite powder) at a pressure of 100 MPa. Thereafter the pellets were sintered in a laboratory furnace in static air at temperature of 1600°C for 4 h with heating rate of 10°C/h.

The thermal behaviour of powder precursors was characterized using Differential Thermal Analysis (DTA) using DTA analyser Netzsch STA 409, where approximately 50 mg of material were put in Pt crucibles and heated at a rate of 10°Cmin^{-1} to 1350°C in a synthetic air flow of 30 cm^{3}min^{-1}. α-alumina was used as a reference material.

The structural analysis was performed by powder X-ray diffraction (XRD) on diffractometer Philips 1830 with CuKα radiation. Data were collected between 10 and 70^o 2θ in a step scan mode with steps of 0.02^o and counting time of 10 s.

Morphology and chemical composition were observed by transmission electron microscope (TEM JEOL 2011) equipped with an energy dispersive X-ray spectrometer (EDS Oxford LINK ISIS). The specimens were prepared by typical ion-milling procedure using an ion-miller (PIPS 691 Gatan Co., USA).

Microstructure of the sintered samples was observed by Scanning Electron Microscopy (SEM) on TESCAN, VEGA TSS 136LS. Previous to analysis, samples were polished and thermally etched at 1550°C for 30 min. thereafter they were coated with gold.

The chemical corrosion behaviour of sintered pellets was investigated by first placing the specimens into a sealed polypropylene (PP) tubes containing 10 mL of HNO_3 solution of several concentrations;0.3 moldm^{-3}, 0.9 moldm^{-3} and 1.5 moldm^{-3}. The static corrosion tests were carried out simultaneously at room temperature (25°C), while the characterisations were conducted 48, 96, 144, 192 and 240 hours upon of immersion. The solution was occasionally stirred to avoid an enrichment of leached components at the surface of samples. After the exposure, the specimens were removed from the tubes, rinsed with boiling distilled water, dried in a laboratory furnace heated at 150°C.

Eluted Al^{3+} and Si^{4+} ions amounts was determined using inductively coupled plasma-optical emission spectrometry (ICP-OES, Thermo Duo Iris Intrepid). Obtained results are expressed as the amount of eluted ions (M^{n+}) in μg per square centimetre of test sample area (μg M^{n+} cm^{-2}). All data were an average of three values.

3. RESULTS SECTION

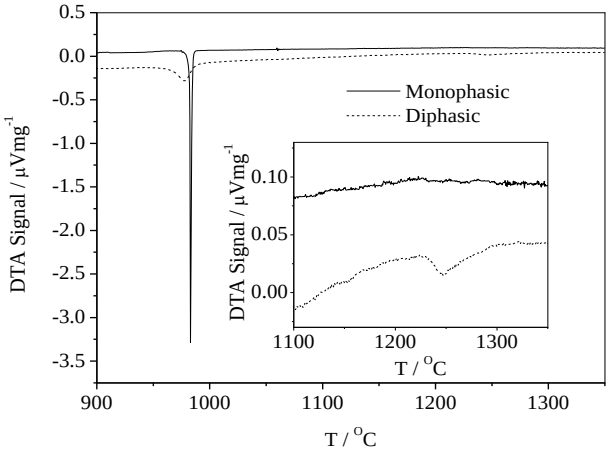

Figure 1. DTA curves of calcined monophasic and diphasic premullite gels. Inset: enlarged segment of DTA curve.

DTA scans of monophasic and diphasic gels are shown in Figure 1. Strong exotherm on DTA curve at ~980°C is attributed to formation of mullite from monophasic premullite gels. In that case this is the sole high-temperature effect. In the case additional small exotherm (Figure 1.) is recorded at higher temperatures [18], then we are evidencing the mullite crystallisation from diphasic premullite gels. Then the first exotherm, evidenced at ~980°C, is actually the crystallisation of the intermediate spinel phase. According to DTA scans the synthesis indeed resulted with the preparation of monophasic and diphasic gel. XRD analysis of the investigated samples thermally treated at 1000°C and 1600°C for 2 h (Figure 2.) provided further evidences on gel type. As can be seen after thermal treatment at 1000°C mullite (ICDD PDF#79-1454), with just a minor amount of Al-Si spinel (ICDD PDF#10-0425), crystallized from monophasic gel. After thermal treatment at 1600°C the diffraction lines of mullite get stronger, spinel lines disappear while traces of α-alumina (ICDD PDF No. 46-1212) diffraction lines appear in XRD patterns.

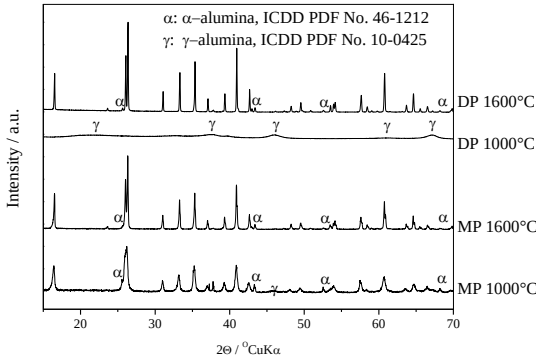

Figure 2. Powder X-ray diffraction patterns of samples of monophasic (MP) and diphasic (DP) gels annealed at 1000°C and 1600°C for 4 h. α – α-alumina, γ - Al-Si spinel (having γ-alumina structure). Unmarked peaks belong to mullite.

On the other hand, in diphasic gels, the intermediate Al-Si spinel which crystallized at about 1000°C, transforms to mullite at higher temperatures. Again, traces of α-alumina appear in XRD patterns. DTA and XRD measurements confirmed the type; monophasic and diphasic, of both gels.

The TEM micrograph of diphasic sample is shown in Figure 3. The micrograph is characterized by both, elongated and equiaxial mullite grains. Such microstructure is characteristic for liquid phase sintering process [19-20]. The presence of small amounts of residual glassy phase was observed, located along the grain boundaries or as glassy-pockets at junctions between mullite grains. The occurrence of SiO_2-rich glassy phase [21] is compositionally compensated with occurrence of alumina-rich phase (α-alumina traces). The mean composition of the glassy phase in diphasic sample, investigated using EDS, was found to be 12.6 mol% Al_2O_3 and 87.4 mol% SiO_2, which is in good accordance with results obtained by Tkalčec et al. (6–12 mol% of Al_2O_3) [22] and Kleebe et al. (10 mol% of Al_2O_3) [23].

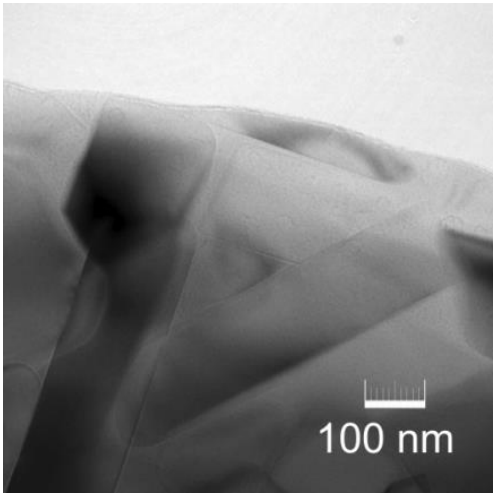

Figure 3. TEM micrograph of diphasic mullite sample sintered at 1600°C.

To evaluate the corrosion behaviour, the amount of cations (Si and Al) released in the corrosive solutions was measured by ICP-OES. The mass of material originating from a unit area of the dissolving solid as a function of time bring about the dissolution rate. Therefore, the corrosion results are given in Figure 4. as a mass of eluted ions from unit areas of pure and doped sample, respectively, as function of corrosion time. The corrosion susceptibility (the amount of eluted ions) increased with corrosion time increase. The trends for the release of Si^{4+} and Al^{3+} are similar for the whole temperature range. As can be seen, for both samples and for all concentrations of HNO_3 solutions, the amounts of leached Si^{4+} are marginally lower than amounts of leached Al^{3+}. The amounts of both ions slightly increases with the increase of HNO_3 concentration. The later increase is more pronounced for samples immersed in 0.9 M HNO_3 solution compared to samples immersed in 0.3 M HNO_3 solution. Obtained results could be clearly apprehended by conversion of leached-ions-amounts to atomic percent. In Table 1. the atomic percent of ionic species leached from pure and doped samples immersed in 1.5 M HNO_3 solution can be observed.

Congruent corrosion of crystalline mullite should yield eluted ions in ratios close to mullite composition, which is not the case here. If one compare weight percent of leached species with the nominal composition it becomes clear that the percent of Si^{4+} ions leached from both samples, monophasic and diphasic-gel derived mullite ceramics, is clearly higher than the nominal percent of Si^{4+} ions in samples resembling to stoichiometric 3:2 mullite (atomic ratio Si:Al = 3:1). Therefore, the percentage presented in Table 2. points out to a glassy phase corrosion. Namely the glassy phase is more sensitive to acid attack than the crystalline phase. On the other hand, the eluate is richer in aluminium compared to glassy phase composition which points out to either crystal phase (selective) dissolution or selective leaching of the glassy phase. Aluminium oxide reacts with water under both acidic and alkaline conditions, i.e., the material is amphoteric [24]. Under neutral pH the solubility is low, however below pH 4 and above pH 9 the solubility increases [25]. However, some investigation of alumina ceramics corrosion in acids [26-27] showed that the process could be attributed mainly to grain boundary impurities. On the other hand, literature data [28] point out to a possibility of migration of aluminium from mullite to acid solution. So we can consider the species leached from the samples (Table 2.) to mainly be the consequence of glassy phase corrosion additionally with some limited crystal phases corrosion, too.

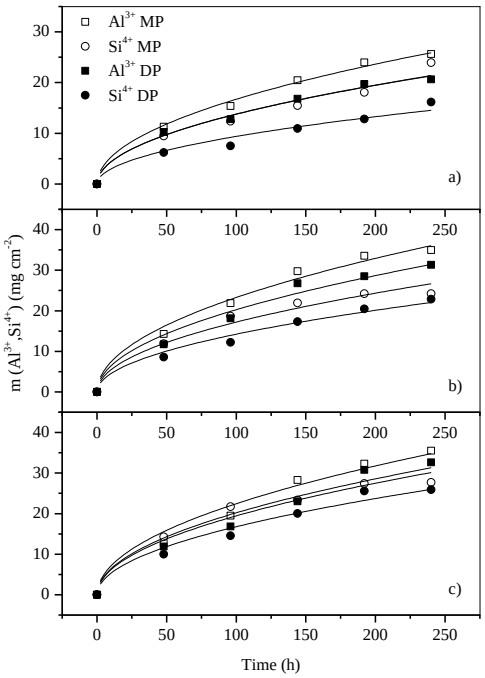

Figure 4. Eluted ions of Al^{3+} and Si^{4+} (mass per unit of surface), from samples of monophasic and diphasic gel derived mullite ceramics, as function of corrosion time: a) in 0.3 M HNO_3 solution, b) 0.9 M HNO_3 solution and c) 1.5 M HNO_3 solution.

Table 1. Percent of species leached from samples which were immersed in 1.5 M HNO_3 solution after 240 h.

Species	Al (at. %)	Si (at. %)
Monophasic-gel derived mullite	56.18	43.82
Diphasic-gel derived mullite	55.73	44.27
Nominal composition	75.00	25.00

Table 2. The parabolic (K_p) corrosion rate constants for samples of mullite ceramics derived from monophasic and diphasic gel immersed in different concentrations of HNO_3 solutions at 25°C.

c(HNO_3) moldm^{-3} (M)	Monophasic		Diphasic	
	K_p / μg^{2}cm^{-4}h^{-1}	R^2	K_p / μg^{2}cm^{-4}h^{-1}	R^2
0.3	9.31	0.9800	5.35	0.9753
0.9	16.39	0.9616	11.90	0.9562
1.5	17.56	0.9870	13.67	0.9330

The corrosion of silicate glasses in aqueous solutions can be governed by leaching (ion exchange) and glass network dissolution via hydration and hydrolysis [29,30]. Corrosion mechanism depend on the pH of contacting solution, where the rate of ion exchange decreases with pH, while the rate of hydrolytic-based dissolutions increases with pH [30-32]. Leaching involves replacement of ions in the glass by a hydronium (H_3O^+) ion from the solution and causes an ion-selective depletion of near surface layers. Leaching is controlled by diffusion and gives an inverse square root dependence of corrosion rate with exposure time (parabolic corrosion kinetic) [33]. On the contrary, glass network dissolution causes a congruent (non-selective) release of ions into the water solution yielding with linear corrosion kinetics [34].

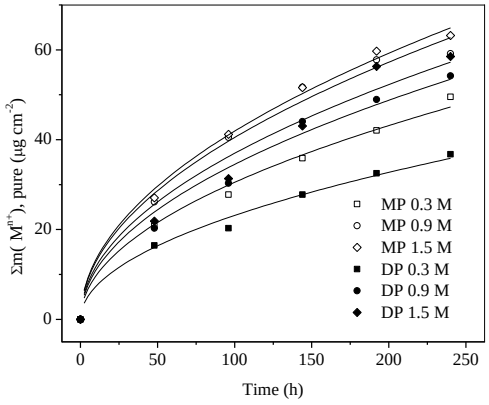

Figure 5. Total amount of eluted ions from unit area of samples of mullite ceramics derived from monophasic and diphasic gel, as function of corrosion time, in various concentrations of HNO_3.

Figure 5. demonstrates the corrosion behaviour of mullite-ceramics samples, derived from monophasic and diphasic gel, showing the mass sum of eluted ions from unit area of samples as a function of corrosion time, immersed in solutions with various concentrations of HNO_3,. Slightly higher corrosion rate is observed for monophasic gel-derived samples in comparison with the diphasic samples. Thereof, the chemical resistance of ceramic is not only the function of chemical composition, but also depends on microstructure, particularly porosity. The diphasic powders could be sintered to a higher density in comparison with the monophasic powders [35]. Therefore, monophasic gel derived mullite ceramics often resemble to high residual porosity enabling penetration of corrosion medium. Consequently, the corrosion resistance of this material is slightly lower. In Figure 6. SEM micrographs of samples sintered from monophasic and diphasic gels at 1600°C are shown. As can be seen sample obtained from monophasic gel is indeed characterized with higher porosity. Corrosion occurs at the boundary of ceramic material with the aggressive environment. Higher porosity leads to greater boundary which further intensifies the corrosion process.

According to Figure 5. parabolic corrosion kinetics of samples could be assumed and thereof corrosion kinetic relations can be expressed using the parabolic law as often used in corrosion data processing [33]: $\Sigma m(M^{n+})=(K_p t)^{1/2}$, where $\Sigma m(M^{n+})$ is the sum of the amount of eluted ions, both Al^{3+} and Si^{4+}, per unit area in μg cm^{-2}, where K_p is the parabolic corrosion rate constant in μg^{2}cm^{-4}h^{-1} and t is time of immersion in h. Power fits having high correlation coefficients are given as lines in Figure 5. Parabolic corrosion rate constants obtained by fitting are given in Table 2. The main influence on chemical corrosion behaviour occur as a consequence of both samples having partially amorphous nature. The process of the glass dissolution is composed of diffusive part where mobile ions move outward through the depleted leach layer, and of the dissolution of the leach layer itself [33]. Thereof, parabolic corrosion kinetics and low corrosion rate occur as consequences of presence of a minute amount of glassy phase. Additional factor is the build-up of a surface leached layer which overall retards the corrosive process of the material underneath. Glassy phase is contains more silicon compared to nominal composition of both samples and thereof prone to chemical attack, while mullite crystalline structure displays better acid-corrosion resistance.

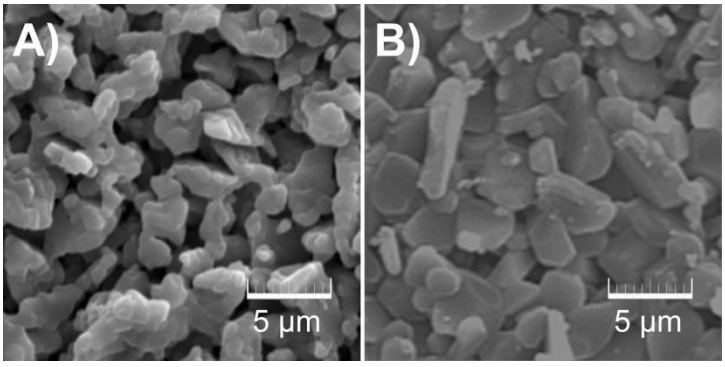

Figure 6. SEM micrographs of samples sintered from gels: a) monophasic gel derived ceramics, b) diphasic gel derived ceramics.

4. CONCLUSIONS

The process of the monophasic and diphasic sol-gel derived premullite-gels development and thermal transformation to mullite ceramic was monitored. The occurrence of glassy phase (predominately in ceramics originating from diphasic gel) was corroborated by TEM observations and its composition was determined using EDS spectrometry. The properties of the corrosion process of mullite ceramics in solution of nitric acid in various concentrations were investigated and compared. The monitoring of corrosion was conducted by monitoring of the concentrations of eluted ions. The corrosion was proportional to the duration of treatment and the concentration of acid solution. Both samples are characterized with low corrosion rates, parabolic

corrosion kinetics and higher Si^{4+}/Al^{3+} ratio in eluate in comparison with nominal composition. Such behaviour was attributed to the corrosion controlled by the glassy phase leaching. Microscopy confirms that mullite ceramics originating from monophasic gel showed greater porosity. Lower corrosion rates of ceramics prepared from diphasic premullite gels has been attributed to lower porosity of those samples.

5. REFERENCES

[1] Schneider H., Schreuer J., Hildmann B., Structure and properties of mullite – A review, *Journal of European Ceramic Society*, 28, 2, 329–344, **2008**.

[2] Hong S.H., Messing G.L., Development of textured mullite by templated grain growth, *Journal of American Ceramic Society*, 82, 4, 867–872, **1999**.

[3] Osendi M.I., Baudin C., Mechanical properties of mullite materials, *Journal of European Ceramic Society*, 16, 2, 217–224, **1996**.

[4] Mazdiyasni K.S., Brown L.M., Synthesis and mechanical properties of stoichiometric aluminium silicate (mullite), *Journal of American Ceramic Society*, 55, 11, 548–52, **1972**.

[5] Schneider H., Saruhan B., Voll D., Merwin I., Sebald A., Mullite precursor phases, *Journal of European Ceramic Society*, 11, 1, 87–94, **1993**.

[6] Winterhalter F., Medri V., Ruffini A., Bellosi A., Corrosion of Si_3N_4-$MoSi_2$ ceramic composite in acid- and basic-aqueous environments: surface modifications and properties degradation, *Applied Surface Science*, 225, 1, 100–115, **2004**.

[7] Sundaresan S., Aksay I.A., Mullitization of diphasic aluminosilicate gels, *Journal of American Ceramic Society*, 74, 10, 2388–2392, **1991**.

[8] Schneider H., Komarneni S., *Mullite*, Wiley-VCH, **2005**.

[9] Krasnyi B.L., Tarasovskii V.I.P., Rakhmanova E.V., Bondar V.V., Chemical resistance of ceramic materials in acids and alkalis, *Glass Ceramics*, 61, 9-10, 337–339, **2004**.

[10] Ueno S., Doni Jayaseelan D., Kondo N., Ohji T., Kanzaki S. Water vapour corrosion of mullite containing small amount of sodium, *Ceramics International*, 31, 1, 177–180, **2005**.

[11] Ueno S., Ohji T., Lin H.-T., Corrosion and recession of mullite in water vapour environment, *Journal of European Ceramic Society*, 28, 2, 431–435, **2008**.

[12] Schmucker M., Mechnich P., Zaefferer S., Schneider H., Water vapour corrosion of mullite: Single crystals versus polycrystalline ceramics, *Journal of European Ceramic Society*, 28, 2, 425–429, **2008**.

[13] Fritsch M., Klemma H., Herrmann M., Schenk B., Corrosion of selected ceramic materials in hot gas environment, *Journal of European Ceramic Society*, 26, 16, 3557–3565, **2006**.

[14] Iwai S., Watanabe T., Minato I., Okada K., Morikawa H., Decomposition of mullite by silica volatilization, *Journal of American Ceramic Society*, 63, 1-2, 44–46, **1980**.

[15] Serhat Baspinar M., Kara F., Optimisation of corrosion behaviour of mullite refractories against alkali vapour via $ZrSiO_4$ addition to the binder phase, *Ceramics*-Silikáty, 53, 4, 242–249, **2009**.

[16] Jacobson N.S., Lee K.N., Yoshio T, Corrosion of mullite by molten salts, *Journal of American Ceramic Society*, 79, 8, 2161–2167, **1996**.

[17] Takahashi J., Kawai Y., Shimada S., Hot corrosion of cordierite/mullite composite by Na-salts, *Journal of European Ceramic Society*, 22, 12, 1959–1969, **2002**.

[18] Schneider H., Okada K., Pask J., *Mullite and Mullite Ceramics*, Wiley, **1994**.

[19] Kanka B., Schneider H., Sintering mechanisms and microstructural development of coprecipitated mullite, *Journal of Materials Science*, 29, 5, 1239–1249, **1994**.

[20] Ivankovic H., Tkalčec E., Nass R., Schmidt H., Correlation of precursor type with densification behaviour and microstructure of sintered mullite ceramics, *Journal of European Ceramic Society*, 23, 2, 283–292, **2003**.

[21] Kong L.B., Zhang T.S., Ma J., Boey F., Anizotropic grain growth of mullite in high-energy ball milled powders doped with transition metal oxides, Zhang R.F., *Journal of European Ceramic Society*, 23, 13, 2247–2256, **2003**.

[22] Tkalčec E., Nass R., Krajewski T., Rein R., Schmidt H., Microstructure and mechanical properties of slip-caste sol-gel derived mullite ceramics, *Journal of European Ceramic Society*, 18, 8, 1089–1099, **1998**.

[23] Kleebe H. J., Hiltz G., Ziegler G.J., Transmission electron microscopy and electron energy loss spectroscopy characterization of glass phase in sol-gel derived mullite, *Journal of American Ceramic Society*, 79, 10, 2592–2600, **1996**.

[24] Shriver D.F., Atkins P.W., Langford C.H., *Inorganic chemistry*, 2nd ed., Oxford University Press, **1994**.

[25] Wefers K., Nomenclature, Preparation, and Properties of Aluminum Oxides, Oxide Hydroxides, and Trihydroxides, in: *Alumina Chemicals*, L.D. Hart, Ed., American Ceramic Society, **1990**.

[26] Mikeska K.R., Bennison S.J., Grise S.L., Corrosion of ceramics in aqueous hydrofluoric acid, *Journal of American Ceramic Society*, 83, 5, 1160–1164, **2000**.

[27] Ćurković L., Fudurić Jelača M., Kurajica S., Corrosion behaviour of alumina ceramics in aqueous HCl and H_2SO_4 solutions, *Corrosion Science*, 50, 3, 872–878, **2008**.

[28] Grum-Grzhimailo O.S., Acid stability of mullite, *Glass and Ceramics*, 31, 7, 479-481, **1974**.

[29] Varshneya A.K., *Fundamentals of inorganic glasses*, Society of Glass Technology, **2006**.

[30] Bunker B.C., Molecular mechanisms for corrosion of silica and silicate glasses, *Journal of Non-Crystalline Solids*, 179, 300–308, **1994**.

[31] Ojovan M.I., Lee W.E., *New Developments in Glassy Nuclear Wasteforms*, Nova Science Publishers, **2007**.

[32] Cailleteau C., Angeli F., Devreux F., Gin S., Jestin J., Jollivet P., Spalla O., Insight into silicate-glass corrosion mechanism, *Nature Materials*, 7, 978–983, **2008**.

[33] White W.B., Theory of Corrosion of Glass and Ceramics, in: *Corrosion of Glass, Ceramics and Ceramic Superconductors*, Eds. Clark D.E., Zoitos B.K., William Andrew Publishing/Noyes, **1992**.

[34] Rana M.A., Douglas R.W., The reaction between glass and water: Part I. Experimental methods and observations, *Physics and Chemistry of Glasses*, 2, 179–205, **1961**.

[35] Hyatt M.J., Bansal N.P., Phase transformations of xerogels of mullite composition, Journal of Materials Science, 25, 6, 2815–2821, **1990**.

6. ACKNOWLEDGEMENTS

The financial support of the University of Zagreb is gratefully acknowledged.

© 2017 by the authors. This article is an open access article distributed under the terms and conditions of the Creative Commons Attribution license (http://creativecommons.org/licenses/by/4.0/).